SIMULATION OF AN IMPINGING JET ISSUED INTO A CROSS FLOW WITH RANS AND LES METHODS

*[1]Rongguang Jia, [2]Johan Revstedt, [2]Rong Ding, [1]Masoud Rokni, [1]Bengt Sundén, and [2]Laszlo Fuchs

[1] Division of Heat Transfer,
Lund Institute of Technology,
P.O. Box 118, 221 00 Lund, Sweden

[2] Division of Fluid Mechanics,
Lund Institute of Technology,
P.O. Box 118, 221 00 Lund, Sweden

*Corresponding author: Rongguang.Jia@vok.lth.se

ABSTRACT

Simulation of the fluid flow and heat transfer of an impinging axi-symmetric jet exiting perpendicular into a cross flow is carried out. Basicly, two methods are employed to model the physics of turbulence: one is by solving the Reynolds averaged Navier Stokes equations (RANS); the other is by the large eddy simulation (LES). In the RANS method, a linear eddy viscosity model (AKN, Abe et al., 1994), an explicit algebraic stress model (EASM, Rokni 2000), and a V2F model Durbin (1995) are employed to close the time averaged momentum equations. The nozzle-to-wall distance (H) is kept at four nozzle diameters (D), while the span-wise width of the channel is 8D. Three ratios (M) of cross flow to jet velocity are considered (0, 0.1, 0.2) for a jet Reynolds number (Re_j) of 20,000. The field data from the RANS and LES methods are compared in detail. In addition, both the calculated heat transfer and fluid flow data are compared with available experimental data.

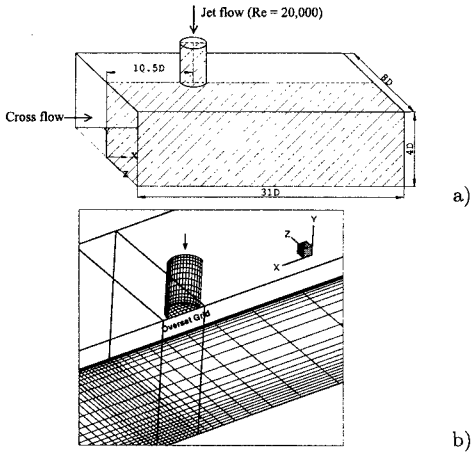

Figure 1: Geometry: a) geometry, b) computation grid.

INTRODUCTION

A jet in cross flow with or without an impingement wall is important both in engineering and in fundamental fluid dynamics, and thus it has been studied extensively over the past half century. Practical applications relate to turbine combustor cooling (impingement and/or film cooling) and air-fuel mixing, pollutant dispersal from chimneys and fires.

Considerable efforts have been spent in studying a jet issued into a cross flow without impingement, both experimentally (Fearn and Weston (1974), Moussa (1977), Fric and Roshko (1994), and Behrouzi and McGuirk (1998)) and numerically (Sykes, et al. (1988), Rudman (1996)). The main phenomena observed in the jet in cross flow are roll-up of coherent vortex rings due to Kelvin-Helmholtz instability in the jet shear layer, formation of the counter-rotating bound vortex pair downstream the jet exit, a horseshoe vortex system in the cross-flow boundary layer upstream the jet exit, and the creation of wake vortices similar to those observed in the flow past a bluff body. The wake system is the least understood system in the jet in cross flow.

However, much less attention has been paid to the impinging jet in cross flow compared to that without impingement. This is often found in application at heat transfer enhancement, e.g., cooling of turbine combustor walls, where the cross-flow may be formed by initial or upstream spent air because the impinged jets must flow to the exit. Due to the existence of the impingement wall, a stagnation region is formed at a high injection ratio. At a low inject ratio, the jet is lifted away from the wall by the cross-flow, so that no obvious stagnation region is observed, which means the influence of the impingement wall will be very small and the structure of the flow field is very similar to that without an impingement wall. For a high injection ratio, only a handful of investigations have been performed experimentally (Oladiran (1981), and Nakabe et al. (1997)), and numerically (Abdon and Sundén (2001)). The latter pointed out insufficiencies of the two-equation models in predicting the heat transfer on the impingement wall.

In addition to a single impingement jet issued into cross-flow, several experimental studies have been carried out on jet arrays, where the cross-flow is formed by initial (Florschuetz et al. 1984) or upstream spent air (Metzger et al. 1979, and Rhee et al. 2003). These studies are focused on the heat transfer on the impingement wall. In the study of Rhee et al. (2003) there is a remarkable increase of stagnation heat transfer due to the presence of cross-flow, which is attributed to the enhanced turbulence intensity of the impinging jets due to the cross-flow disturbance. However, a contradictory result was observed by Metzger et al. (1979). On the other hand Florschuetz et al. (1984) reported

that the addition of the initial cross-flow resulted in reduced mean Nusselt number (Nu), but for small jet-to-wall distances, e.g., $H/D = 1$, the cross-flow will enhance the mean heat transfer coefficients. Due to the difficulties in modelling the turbulence, numerical works on jet array impingement are relatively few. In the numerical study of impingement cooling of a two-pass channel by Jia et al. (2003), decent agreement with experiments was obtained for the average Nu by using the V2F model. However, validation of the predicted detailed local values is necessary before stepping further. This constitutes one of the aims of this study.

In this study, both RANS and LES methods are employed to test their ability in predicting such kind of fluid flow and heat transfer problems.

METHODS

Three-dimensional steady and unsteady simulations were carried out by the RANS and LES methods, respectively.

RANS Method

In the RANS method, the AKN, EASM, and V2F turbulence models are employed to close the time averaged momentum equations, and the energy equation is closed by the simple eddy diffusivity (SED) model. Details can be found in Jia et al. (2002).

The RANS computations are carried out in an in-house multi-block parallel computer code CALC-MP (Jia and Sundén, 2003), based on the finite volume technique. The code uses a collocated body-fitted grid system and employs the improved Rhie and Chow interpolation to calculate the velocities at the control volume faces. The SIMPLEC algorithm couples the pressure and velocity. An algorithm based on SIP is used for solving the algebraic equations. Coefficients are determined by the QUICK scheme for the momentum equations and hybrid scheme for all the other discretized equations. In the present simulation, a rectangular grid is used for the channel, and a body fitted grid for the jet pipe, as shown in Fig. 1b. A trilinear interpolation method is employed to achieve the connectivity. An investigation of grid dependence has been carried out to find the final proper mesh, $154 \times 73 \times 68$.

LES Method

For LES, an implicit SGS model is employed for both the momentum and scalar transport. In the computational code used the convective terms are approximated by third order upwind finite differences. The truncation error from this approximation acts dissipatively, at least in an averaged sense, draining energy from the resolved scales. It was shown by Olsson and Fuchs (1994) for a free jet that this term is of the same order and located in the same area as the SGS-term in a Smagorinsky model. However, it should be noted that for a given grid, the resolution of the turbulent properties are improved by using explicit SGS models, e.g., Revstedt *et al.* (1998).

The LES simulations are achieved in a parallel code using a Cartesian staggered grid. The spatial discretisation of the governing equations is performed on a Cartesian staggered grid. The convective terms are discretised using the third order upwind scheme by Rai and Moin (1991). A fourth order central difference scheme was used for all other terms (Olsson and Fuchs, 1998). Time integration is done by a four step explicit Runge-Kutta type scheme. A Poisson equation is solved for the pressure correction. To accelerate the solution of this equation a multi grid method is used.

The transport equation for concentration is solved only on the finest multi-grid level by using a converged velocity field. It is discretised using the same scheme as for the momentum equations. However, in order to avoid unphysical oscillations in the solution, the spatial discretisation is switched to a lower order scheme if the limits of maximum and minimum concentration are exceeded.

The computational domain for LES is rectangular and the size is $16D \times 4D \times 8D$. The jet inlet is placed $6D$ from the cross flow inlet. The number of grid points on the finest multi-grid level is $384 \times 96 \times 194$.

Boundary Conditions

For the RANS simulation, both the jet and the cross flows (including the turbulent components) are set as the fully developed flow inlets, while a "top-hat" profile is applied for both of the inlet in the LES computation. In LES, a random perturbation of 5% of the average inlet velocity was superimposed on the nozzle velocity in all directions. Three ratios of cross flow to jet velocity are calculated (0, 0.1, 0.2), while only the case with $M = 0.1$ is computed with LES. In all the cases, the jet Re (Re_j) is kept constant at 20,000.

The inlet temperatures for the jet inlet and cross-flow inlet are set as a constant (T_{in}) in the RANS simulation, while in the LES method, the jet inlet temperature is set as T_{in} and the cross-flow temperature is set as the same as the impingement wall temperature T_w.

At the impingement wall, a constant heat flux q_w boundary condition is used for the RANS method while a constant temperature T_w for the LES method, while all the other walls are set as adiabatic. The no-slip boundary condition is set as:

$$U_w = 0, \quad V_w = 0, \quad W_w = 0 \tag{1}$$

$$k_w = 0, \quad \epsilon_w = 2\frac{\nu k_1}{y_1} \tag{2}$$

$$\overline{v_w^2} = 0, \quad f_w = -\frac{20\nu^2\overline{v_1^2}}{\epsilon_w y_1^4} = -\frac{10\nu}{y_1^2} \cdot min(\frac{\overline{v_1^2}}{k_1}, 2) \tag{3}$$

where indices w and 1 denote the wall and the first point off the wall, respectively.

At the outlet a Neumann condition corrected to ensure global mass conservation is applied.

Computation of the Nu

For a constant heat flux (q_w) wall boundary one has:

$$Nu = \frac{\alpha D_h}{\lambda} = \frac{q_w D_h}{\lambda(T_w - T_b)} \tag{4}$$

For a constant temperature (T_w) wall boundary one has:

$$Nu = \frac{\alpha D_h}{\lambda} = \frac{D_h(T_w - T_1)}{y_1(T_w - T_b)} \tag{5}$$

where indices w and 1 denote the wall and the first point off the wall, respectively.

A test on the method of calculating the reference temperature is also carried out, as shown in Fig. 4b. The solid line shows the $T_{ref} = T_{in}$ method, which is also used in the experiments. However, if the bulk temperature $T_b = \frac{\dot{Q}}{\rho V_{in} c_p} \frac{r^2}{R^2} + T_{in}$ is used for the reference temperature T_{ref}, the results will be as the dotted line in Fig. 4b. The relation between the two methods is as follows:

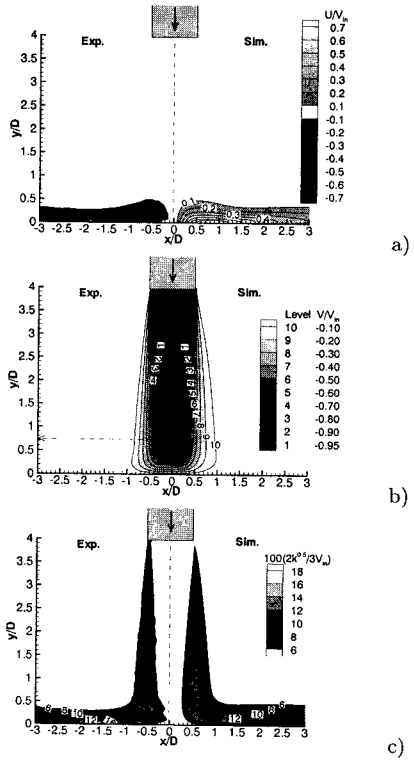

Figure 2: Comparison with the PIV experiments $Re = 23,000$, $H/D = 4$: a) U-velocity, b) V-velocity, c) turbulent kinetic energy

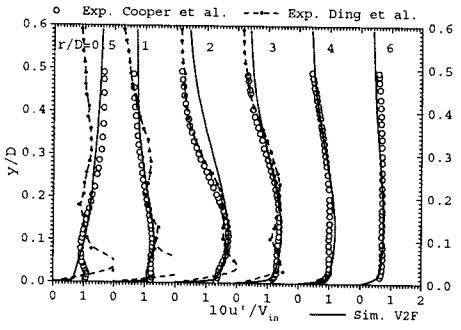

Figure 3: The comparison of the rms velocity parallel to the wall

$$Nu = \frac{1}{1 - \frac{r^2}{R^2}\frac{Nu'}{RePr}} Nu' \qquad (6)$$

where Nu' denotes the Nu based on the jet inlet temperature T_{in}, and r is the distance from the impingement center. It is obvious that the usage of the real bulk temperature in calculating the Nu number in a higher Nu.

PROBLEM STATEMENT

The considered case is a round jet impinging on the bottom wall of a channel with a rectangular cross-section, as shown in Fig. 1a, where the dimensions are also shown. The whole channel is selected as the computation domain in LES excluding the jet pipe, while only half is selected for RANS computations including the jet pipe.

RESULTS & DISCUSSION

Due to the lack of detailed experimental data for the impingement with cross-flow cases, the solver and turbulence models are first validated versus a circular impinging jet without cross-flow $H/D = 2$ and 4, $Re = 23,000$. Then the impinging jet with cross-flow rates $M = 0.1$ and 0.2 are studied by the validated solver.

A circular jet without cross-flow

Fig. 2a shows the calculated (right) U-velocity contours compared with those from experiments by Ding (2003). Very good agreement is observed. In addition, at the stagnation region, the acceleration of the fluid is very fast, which means that one of the normal strains is very big.

Fig. 2b shows the V-velocity contours. Generally speaking, the agreement is good. However, the spread of the computational results seems faster than the experimental ones. This might be due to the over-prediction of the turbulence in the mixing layer, as shown in Fig. 2c. The over-predicted turbulence intensity makes the spreading faster, or entrains more of the surrounding fluids. In addition, the predicted potential core length is a little longer than in the experiments ($3.25D$). This could be attributed to that in the calculations there is a confined wall, but not in the experiments.

Fig. 2c shows the turbulent kinetic energy contours. The agreement of both the shape and level is good. The largest difference is at the stagnation region, where the shape is quite different. This region is very close to the wall. Probably, higher resolution is necessary for the PIV system here, because the flow field is very complex at this region. This will be further explained in the next picture.

Fig. 3 compares the results of normalized fluctuation parallel to the wall from HWA, PIV, and the numerical simulation with the V2F model. The agreement is decently good. Very close to the stagnation region ($x/D = 0.5$), the numerical results are a little lower than the HWA data, while the PIV data are much higher which partly explains the discrepancy of Fig. 2c at the stagnation region. With the development of the wall jet, the agreement between the

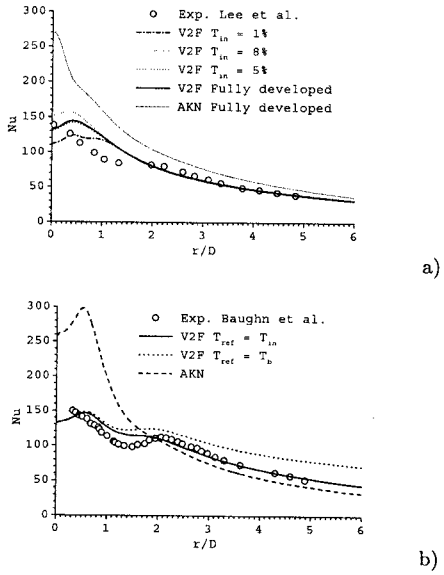

Figure 4: Nu on the impingement wall without cross-flow: a) H/D = 4, b) H/D = 2

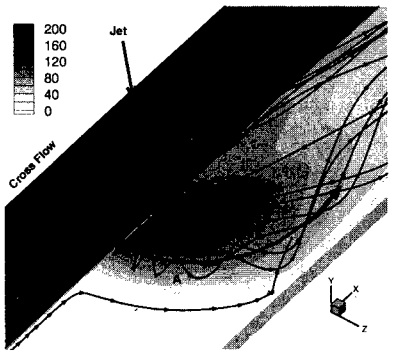

Figure 5: The streamline trace for the M = 0.2 case, and the contours on the impingement wall show the distribution of the Nu,

three methods becomes better. However, at the far-wall region, especially for $r/D = 2$, in consistence with Fig. 2c also, the numerically predicted contours of the kinetic energy is thicker at the wall jet region.

Fig. 4 shows the local Nu on the impingement wall for two jet-to-wall distances. For $H/D = 4$, the numerically predicted results are in pretty good agreement with the experiments of Lee et al (1999). Some effect of the jet inlet boundary conditions for the V2F model is also checked. For the V2F model, the increase of the inlet turbulence intensity generally enhances the heat transfer at the stagnation region. In addition, the flat profile for a turbulence intensity of 5% yields the same results as with the fully developed profile. Concerning this, the fluctuation of the fully developed profile of the experiments by Ding et al. (2003) was checked, and the average of the inlet turbulence intensity was also around 5%. This could partly serve as an explanation. As for the AKN model, the over-prediction at the stagnation region is severe. This is in accordance with the established knowledge, where the large normal strain results in excessive production of turbulence at the stagnation region. Similar results are obtained for the $H/D = 2$ case.

A circular jet with cross-flow

Fig. 5 shows the streamline trace for the $M = 0.2$ case. Two features can be clearly observed. One is the roll-up upstream the jet due to the interaction between the cross flow and jet flow (also shown in Fig. 6); another is the wake flow downstream the jet (also shown in Fig. 7). The upstream roll-up is mainly due to the presence of the impingement wall, while the downstream wake flow is similar to that of a free jet issued into cross flow.

The distribution of the Nu (Fig. 5) is reformed by the cross flow into a kidney shape, which is in coincidence with the shape of the velocity contour (see Fig. 7). If the cross-flow is strong enough, this will be transferred into the counter-rotating vortex system, due to the shear from the cross-flow, instead of impingement on the wall.

Examining the calculated flow features in more detail, Fig. 6 shows the flow structure at the symmetry plane near the jet for two different cross flow rates. With the introduction of the cross-flow, the stagnation region moves downstream ($M = 0.1$). This shift is strengthened by the larger cross flow velocity ($M = 0.2$). Another point is the formation of the recirculation upstream the stagnation region. This recirculation becomes smaller for stronger cross flow rate. The flow field predicted by LES is shown in Fig. 6b with the same cross-flow ratio ($M = 0.1$) as Fig. 6a. The stream-wise location of the upstream vortex center is in good agreement, but the lift-up of the vortex is larger in the LES. This might be because of the difference in the boundary conditions of the two methods. In the LES, a top-hat profile is employed as the cross-flow inlet and the cross-flow inlet is $6.5D$ upstream the jet center, so that a sharper profile prevails from the inlet to the interaction with the upstream wall jet. This stronger interaction, results in a larger roll-up vortex and higher turbulence as shown in Fig. 8b.

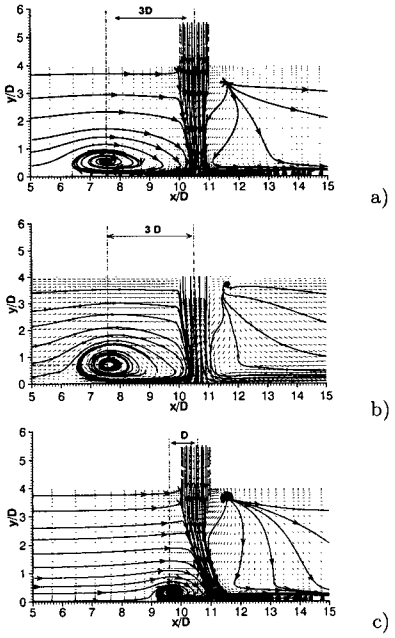

Figure 6: UV plot at the symmetry plane for: a) $M = 0.1$ with V2F, b) $M = 0.1$ with LES, c) $M = 0.2$ with V2F, and the contours are for the V-velocity

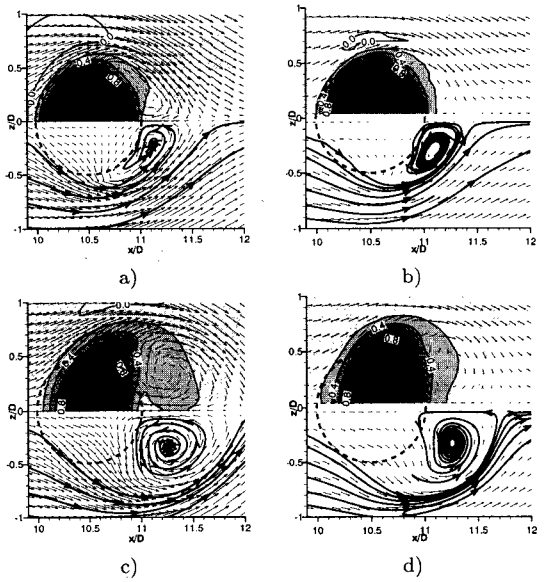

Figure 7: The horse-shoe and wake vortices for the M01 case, a) at $y/D = 3$ (V2F), b) at $y/D = 3$ (LES), c) $y/D = 2$ (V2F), and d) $y/D = 2$ (LES)

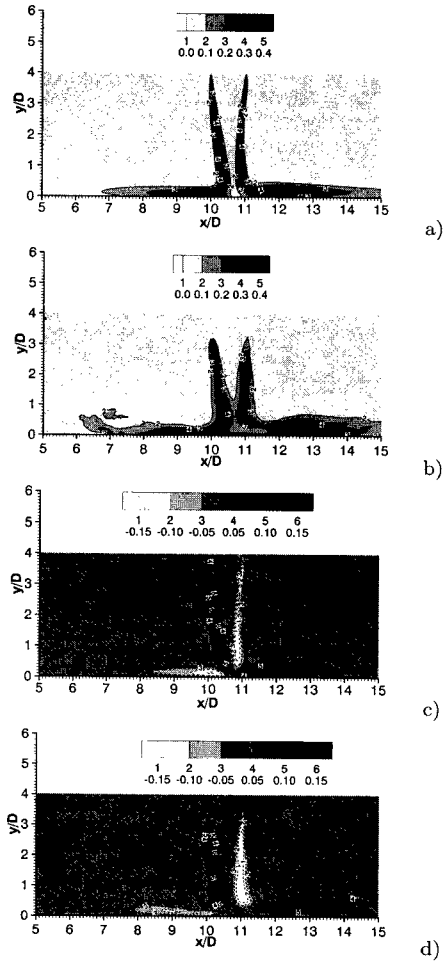

Figure 8: The predicted Reynolds stresses at the symmetry plane for the M01 case, a) $10\frac{\overline{u'u'}}{V_j^2}$ (V2F), b) $10\frac{\overline{u'u'}}{V_j^2}$ (LES), c) $10\frac{\overline{u'v'}}{V_j^2}$ (V2F), and d) $10\frac{\overline{u'v'}}{V_j^2}$ (LES)

Fig. 7 shows the horse-shoe and wake vortices. The horseshoe vortex is located close to the jet exit, and in the cross-flow boundary layer upstream from the jet exit. The creation of wake vortices is similar to observations in flow past a bluff body. They are inherently unsteady, and the unsteadiness is captured by the LES method. The agreement between the two methods is good, notwithstanding the longer wake predicted by RANS. The difference might be partly due to the different inlet boundary conditions. In addition the longer wake may also be because it omits an important component of the averaged flow field, the periodic vortex shedding.

A more critical test of the turbulence model can be made by comparing the turbulence variables. Fig. 8 shows the Reynolds stresses predicted by V2F and LES (statistics from unsteady simulation). Generally speaking, the agreement is good, for both trend and magnitude. However, the mixing layer (defined as the high turbulence layer shear layer) predicted by LES seems to develop later and be thicker. This could be double checked from the comparison between the V2F and the experiments of Ding, as shown in Fig. 2c. The predicted mixing layer by the V2F is in pretty good agreement with the experiments, so the only possible reason

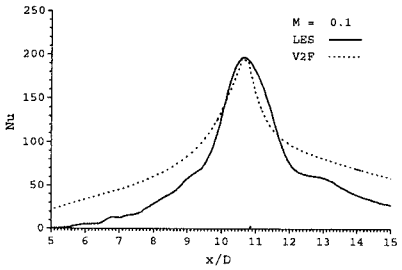

Figure 9: The comparison of the Nu at the symmetry line between the LES and V2F model

for the discrepancy between V2F and LES is the jet inlet boundary conditions. The top-hat jet inlet profile results in a larger velocity gradient at the edge of the jet flow, consequently higher turbulence intensity and more entrainment or a thicker mixing layer. The agreement for the shear stress $\overline{u'v'}$ is better, but the same discrepancy still exists as for $\overline{u'u'}$.

Fig. 9 shows a comparison of the Nu at the symmetry line on the impingement wall between the two methods. The agreement at the stagnation region is quite good. However, at the regions outside the stagnation region, the prediction from the LES model is too low, because the average Nu of a channel flow with a $Re \approx 8,000$ is around 25. The main reason for this is the usage of $T_{in} = T_w$ for the cross-flow inlet in the LES. Actually, Nu indicates the heat transfer capability between a wall and a fluid flow, although it is calculated from the temperature field (the gradient). Therefore, Nu can represent the flow field properly, only if there is a temperature gradient compatible with the flow field. $T_{in} = T_w$ for the cross-flow inlet ruled out this compatibility in the upstream region.

Fig. 10a shows the Nu distribution at the symmetry line on the impingement wall. As shown, all the three RANS models provide pretty similar predictions. The presence of the cross-flow alleviates the over-prediction of turbulence at the stagnation region of AKN and EASM. At the stagnation region, the Nu is much higher with $M = 0.1$ than that with $M = 0$. This is in accordance with the experiments of Rhee et al. (2003), which is attributed to the enhanced turbulence intensity due to the interaction between the cross-flow and jet flow. The increase of the turbulence intensity can be observed from Fig. 10b.

With the increase of the cross flow rate, the downstream shift of the stagnation point (or the maximum Nu) can be observed. This is because the cross-flow will squeeze under the impinging jet, deflecting the jet flow, and weakening the turbulence.

CONCLUSIONS

A study of a circular impinging jet with or without cross-flow has been carried out. For the zero cross-flow case, the results by the V2F model are in good agreement with the experimental data.

The interaction between the cross-flow and jet flow enhances the turbulence intensity of the jet, consequently higher stagnation region heat transfer coefficients appear. However, if the cross-flow is very strong, e.g., $M = 0.2$, the jet flow will be severely deflected, and the heat transfer will be weakened.

The results from the LES computation are in decent good

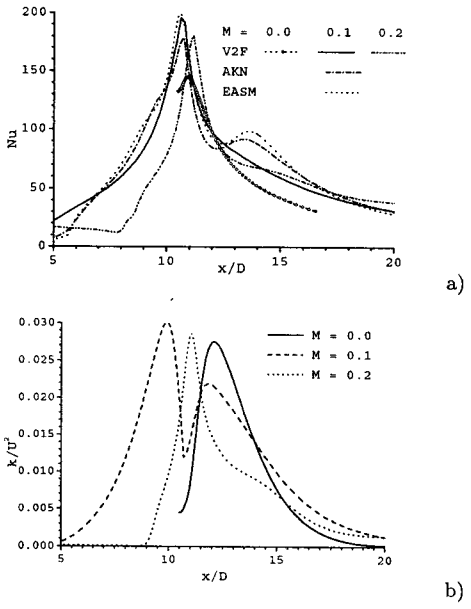

Figure 10: a) Nu distribution at the symmetry line on the impingement wall, b) turbulent kinetic energy distribution at $y/D = 0.2$ and $M = 0.1$

agreement with the present RANS methods.

ACKNOWLEDGEMENTS

This work was financially supported by the Swedish National Energy Agency through the Energy Related Fluid Mechanics programme. Computational resources from the Swedish National Supercomputer Center (project no. p2003049) and from the center for scientific computing at Lund University are also gratefully acknowledged.

REFERENCES

Abdon, A, and Sunden, B. (2001), "Numerical Simulation of Impinging Jet Heat Transfer in the Presence of Crossflow", *ICHMT Computational Heat Transfer Symposium CHT'01*, Australia.

Abe, K., Kondoh, T., and Nagano, Y. (1994), "A New Turbulence Model for Predicting Fluid Flow and Heat Transfer in Separating and Reattaching Flows-I. Flow Field Calculations", *Int. J. Heat Mass Transfer*, 37:1, 139–151.

Baughn, J., Hechanova, A., and Yan, X., (1991), "An Experimental Study of Entrainment Effect on the Heat Transfer from a Flat Surface to a Heated Circular Impinging Jet", *ASME J. Heat Transfer*, 113, 1023–1025.

Behrouzi, P., and McGuirk, J.J. (1998), "Laser Doppler Velocimetry Measurements of Twin-jet Impingement Flow for Validation of Computational Models", *Optics and Lasers in Engineering*, 30, 265–277.

Corrtelezzi, L., and Karagozian, R. (2001), "On the Formation of the Counter-rotating Vortex Pair in Transverse Jets". *J. Fluid Mechanics*, 446, 347–373.

Ding, R. (2003), "Experimental Study of Turbulent Mixing in Impinging Jets", *Licentiate thesis*, Division of Fluid Mechanics, Department of Heat & Power Engineering, Lund Institute of Technology.

Durbin, P.A. (1995), "Separated Flow Components with V2F Model", *AIAA J.*, 33:4, 659–664.

Fearn, R., and Weston, R.P. (1974), "Vorticity Associated with a Jet in a Cross-Flow", *AIAA J.*, 12:3, 1666–1671.

Fric, T.F., and Roshko, A. (1994), "Vortical Structure in the Wake of a Transverse Jet", *J. Fluid Mechanics*, 279, 1–47.

Jones, W.P., and Wille, M. (1996), "Large-eddy Simulation of a Plane Jet in a Cross-flow", *Int. J. Heat Fluid Flow*, 17, 296–306.

Jia, R., Rokni, M., and Sundén, B. (2002), "Numerical Assessment of Different Turbulence Models for Slot Jet Impinging on Flat and Concave Surfaces", *ASME Turbo Expo. GT-2002-30449.*

Jia, R., Rokni, M., and Sundén, B. (2003), "Numerical Investigation of Impingement Cooling in Ribbed Ducts due to Jet Arrays", accepted by *J. Enhanced Heat Transfer.*

Jia, R., and Sundén, B. (2003), "Parallelization of a Multi-Blocked CFD Code via Three Strategies for Fluid Flow and Heat Transfer Analysis", Accepted by *Computers & Fluids.*

Jia, R., and Sundén, B. (2003), "A Multi-Block Implementation Strategy for a 3D Pressure-Based Flow and Heat Transfer Solver", Submitted for publication.

Moussa, Z.M., Trishka, J.W., and Eskinazi, S. (1977), "The near Field in the Mixing of a Round Jet with a Cross-Stream", *J. Fluid Mechanics*, 80, 49–80.

Nakabe, K., Inaoka, K., Ai, T., and Suzuki, K. (1997), "Flow Visualization of Longitudinal Vortices Induced by an Inclined Impinging Jet in a Crossflow-Effective Cooling of High Temperature Gas Turbine Blades", *Energy Conversion and Management*, 38:10-13, 1145–1153.

Oladiran, M.T. (1981), *The effect of nozzle inclination on heat transfer in jet impingement systems*, Ph.D. Thesis, Cranfield Institute of Technology, UK.

Olsson, M., and Fuchs, L. (1994), "Significant Terms in Dynamic Sgs-modeling", *Direct and Large Eddy Simulations I*, P.R. Voke, ed., Kluwer Academic Publishers.

Olsson, M., and Fuchs, L. (1998), "Large Eddy Simulations of a Forced Semiconfined Circular Impinging Jet", *Phys. Fluids*, 10, 476–486.

Rai, M.M., and Moin, P. (1991), "Direct Simulations of Turbulent Flow Using Finite-difference Schemes", *J. Comput. Phys.*, 96:1, 15–53.

Revstedt, J., Gullbrand, J., Guillard, F., Fuchs, L., and Trägårdh, C. (1998), "Large Eddy Simulations of Mixing in an Impinging Jet", *Proc. of the 4th ECCOMAS Computational Fluid Dynamics Conference*, K.D. Papailiou et al., ed., John Wiley & Sons, 1169-1174.

Rhee, D.H. , Yoon, P.H. and Cho, H.H. (2003), "Local heat/mass transfer and flow characteristics of array impinging jets with effusion holes ejecting spent air", *Int. J. Heat Mass Transfer*, 46:6, 1049–1061.

Rokni, M. (2000), "A new low-Reynolds version of an explicit algebraic stress model for turbulent convective heat transfer in ducts", *Num. Heat Transfer Part A*, 37:3, 331–363.

Rudman, M. (1996), "Simulation of the Near Field of a Jet in a Cross Flow", *Experimental Thermal and FLuid Science*, 12, 134–141.

Sykes, R.I., Lewellen, W.S., and Parker, S.F. (1986), "On Vorticity Dynamics of a Tubulent Jet in a Cross-Flow", *J. Fluid Mechanics*, 168, 393–413.